materials

MDPI

Article

Evaluation of Adhesion Properties of Thin Film Structure through Surface Acoustic Wave Dispersion Simulation

Yu Min Choi [1], Dongchan Kang [2], Jeong Nyeon Kim [3] and Ik Keun Park [4,*]

[1] Department of Mechanical Engineering, Graduate School, Seoul National University of Science and Technology, Seoul 01811, Korea
[2] Graduate School of Nano IT Design Fusion, Seoul National University of Science and Technology, Seoul 01811, Korea
[3] Ginzton Laboratory, Stanford University, Stanford, CA 94305, USA
[4] Department of Mechanical and Automotive Engineering, Seoul National University of Science and Technology, Seoul 01811, Korea
* Correspondence: ikpark@seoultech.ac.kr; Tel.: +82-2-970-6332

Abstract: A theoretical simulation study of the dispersion characteristic of the surface acoustic wave (Rayleigh wave) was conducted by modeling the adhesion interlayer with stiffness coefficients to evaluate the bonding properties of nano-scale thin film structures. For experimental validation, a set of thin film specimens were fabricated—637 nm, 628 nm, 637 nm, 600 nm, and 600 nm thick titanium (Ti) films were deposited on silicon (Si) (100) substrate using a DC Magnetron sputtering process with DC power from 28.8 W, 57.6 W, 86.4 W, 115.2 W, and 144 W. The thicknesses of the Ti films were measured using a scanning electron microscope (SEM). Surface acoustic wave velocity for each of the manufactured thin film specimens was measured by using a V(z) curve technique of a Scanning Acoustic Microscope. The measured velocity, transducer frequency, and thickness of the film were applied to dispersion characteristic simulation for a given stiffness coefficient to calculate adhesion strength of each specimen. To verify the simulation result, the adhesion force of each specimen was measured using a nano-scratch test and then compared with the calculated values from the dispersion characteristic simulation. The value of adhesion strength from the dispersion characteristic simulation and the value of adhesion force of the nano-scratch test were found to have a similar tendency according to the process variable of the thin film. The results demonstrated that the adhesion strength of a thin film could be evaluated quantitatively by calculating the dispersion characteristics with the adhesion interlayer stiffness model.

Keywords: V(z) curve technique; dispersion characteristics; adhesion strength; scanning acoustic microscope

check for updates

Citation: Choi, Y.M.; Kang, D.; Kim, J.N.; Park, I.K. Evaluation of Adhesion Properties of Thin Film Structure through Surface Acoustic Wave Dispersion Simulation. *Materials* **2022**, *15*, 5637. https://doi.org/10.3390/ma15165637

Academic Editor: Victor Ralchenko

Received: 11 July 2022
Accepted: 16 August 2022
Published: 16 August 2022

Publisher's Note: MDPI stays neutral with regard to jurisdictional claims in published maps and institutional affiliations.

Copyright: © 2022 by the authors. Licensee MDPI, Basel, Switzerland. This article is an open access article distributed under the terms and conditions of the Creative Commons Attribution (CC BY) license (https://creativecommons.org/licenses/by/4.0/).

1. Introduction

Thin film structures are used in various fields such as semiconductors, displays, and MEMS devices. As the technology advances, the thickness of the thin film becomes smaller on a micro/nano-scale. Research has been conducted to detect various defects and evaluate physical properties. In particular, since the adhesion strength of the thin film directly affects the life and performance of the product, various studies have been conducted to evaluate adhesion strength [1–5]. However, destructive techniques, such as SEM, TEM, nano-indentation test, and nano-scratch test, damage the specimen during pretreatment or measurement, so the specimen cannot be reused [5–7]. On the other hand, nondestructive techniques that use acoustic and optics to evaluate the adhesion strength have a limitation of non-derived quantitative results [2]. A study to increase reliability was conducted by using the destructive technique nano-scratch test and the non-destructive technique AE at the same time [3]. To overcome these limitations, this study was conducted to quantitatively evaluate the adhesion strength of thin films using an acoustic nondestructive

technique. The advantage of non-destructive evaluation using acoustic is that it is possible to evaluate properties by measuring the acoustic velocity with high precision in a small area based on the acoustic–elastic effect, which is the relationship between the acoustic velocity propagating inside the material and the internal/applied stress. Based on this, properties of single and composite materials such as acoustic anisotropy, twin strain, processing change layer, thin film thickness measurement, residual stress, bonding properties, and mechanical properties can be identified [8–12]. For a nondestructive evaluation, the acoustic velocity of the Rayleigh wave was measured by applying the V(z) curve technique of a scanning acoustic microscope. Then, the dispersion characteristics of the surface acoustic wave (*SAW*) in a multilayer structure were simulated to convert the measured sound velocity to adhesion strength. The method of simulating the theoretical dispersion curve was carried out following that of the previous study [13]. In order to evaluate the adhesion properties of thin film, a virtual adhesion interface, having a spring stiffness coefficient between the thin film and the substrate, was modeled. Conducting the dispersion characteristic simulation that includes this modeling, the dispersion characteristics were calculated for the given stiffness coefficient. A titanium thin film was deposited to a silicon substrate using a DC magnetron sputtering process to verify the adhesion strength evaluation method through dispersion characteristic simulation. *SAW* velocity of the manufactured specimens were then nondestructively measured using a V(z) curve technique of the scanning acoustic microscope. The adhesion strength according to physical properties, such as measured sound velocity, the frequency used in the measurement, and the thickness of the thin film, was derived from the dispersion characteristic simulation. In order to verify the reliability of the adhesive strength evaluation method through dispersion characteristic simulation, a nano-scratch test, a commercial adhesive force evaluation technique, was performed on the fabricated specimens and the results were compared.

2. Related Theory

2.1. Dispersion Characteristics of Multilayer Thin Film

The ultrasound propagating through a multilayered thin film structure has a dispersion characteristic, in which the phase velocity changes according to the thickness and frequency of the thin film. To evaluate the dispersion characteristic, a dispersion curve for the thin film and the substrate was derived using Thomson–Haskell's transfer matrix method [14]. The properties of the elastic wave traveling through the multilayered structure are expressed with the displacement–stress equation expressed in terms of amplitude. Applying this to the transfer matrix, the dispersion characteristics for the multilayered structure was calculated. The reliability of the dispersion curve calculated by the transfer matrix method was evaluated through previous studies [14–16].

Figure 1 shows the amplitude parameter through the multi-layered thin film structure. Wave analysis for multi-layer structures is generally performed in a two-dimensional coordinate system, because the wavelength is negligibly small compared to the width of the structure. In the *SAW* traveling through the thin film, only the propagation direction (x) and the depth (z) of the wave are considered and analyzed. In Figure 1, A_L^+ and A_S^+ are the upward longitudinal and transverse wave components, respectively; A_L^- and A_S^- are the downward longitudinal and transverse wave components. Therefore, the displacement vectors of the longitudinal and transverse waves, represented by the scalar function ϕ and the vector function ψ, are as shown in Equation (1) below.

$$\begin{Bmatrix} u_x \\ u_y \\ u_z \end{Bmatrix}_{(L)} = \begin{Bmatrix} \frac{\partial}{\partial x} \\ \frac{\partial}{\partial y} \\ \frac{\partial}{\partial z} \end{Bmatrix} \times \phi = \begin{Bmatrix} k_x \\ 0 \\ k_z \end{Bmatrix} A_L \, e^{i(kx-wt)}$$
$$\begin{Bmatrix} u_x \\ u_y \\ u_z \end{Bmatrix}_{(S)} = \begin{Bmatrix} \frac{\partial}{\partial x} \\ \frac{\partial}{\partial y} \\ \frac{\partial}{\partial z} \end{Bmatrix} \times \psi = \begin{Bmatrix} k_x \\ 0 \\ -k_z \end{Bmatrix} A_S \, e^{i(kx-wt)} \quad (1)$$

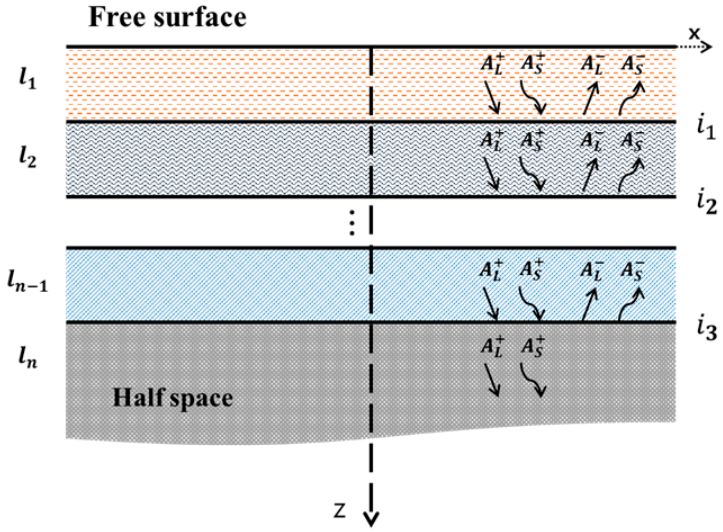


Figure 1. Schematic diagram of *SAW* propagating in multi-layer thin films.

Here, k_x and k_z are the wavenumber in the x-direction and z-direction, respectively, A_L is the amplitude of the longitudinal wave, and A_S is the amplitude of the transverse wave. In the Cartesian coordinate system, the relationship between the displacement, stress, and amplitude in the propagation direction (x-axis) and the depth direction (z-axis) is as shown in Equation (2) below.

$$\begin{Bmatrix} u_x \\ u_z \\ \sigma_{zz} \\ \sigma_{xz} \end{Bmatrix} = \begin{bmatrix} k_x g_\alpha & \frac{k_x}{g_\alpha} & C_\beta g_\beta & -\frac{C_\beta}{g_\beta} \\ C_\alpha g_a & -\frac{C_\alpha}{g_\alpha} & k_x g_\beta & \frac{k_x}{g_\beta} \\ i\rho B g_\alpha & \frac{i\rho B}{g_\alpha} & 2i\rho k_x \beta^2 C_\beta g_\beta & \frac{2i\rho k_x \beta^2 C_\beta}{g_\beta} \\ 2i\rho k_x \beta^2 C_\alpha g_\alpha & \frac{-2i\rho k_x \beta^2 C_\alpha}{g_\alpha} & i\rho B g_\beta & \frac{i\rho B}{g_\beta} \end{bmatrix} \cdot \begin{Bmatrix} A_L^+ \\ A_L^- \\ A_S^+ \\ A_S^- \end{Bmatrix} \quad (2)$$

Here, the amplitude of the ultrasonic wave traveling in the depth direction of the thin film structure is represented by + subscript, and that traveling in the opposite direction is represented by the—subscript. The variables, C_α, C_β, g_α, g_β and B, are arbitrarily designated abbreviations for convenience of calculation and are expressed as follows.

$$\begin{aligned} C_\alpha &= \left(w^2/\alpha^2 - k_x^2\right)^{1/2} \\ C_\beta &= \left(w^2/\beta^2 - k_x^2\right)^{1/2} \\ g_\alpha &= e^{i\left(w^2/\alpha^2 - k_x^2\right)^{1/2} z} \\ g_\beta &= e^{i\left(w^2/\beta^2 - k_x^2\right)^{1/2} z} \\ B &= w^2 - 2\beta^2 k_x^2 \end{aligned} \quad (3)$$

The 4×4 matrix in Equation (2) is defined as a coefficient matrix $[D]$, which represents the relationship between displacement–stress and amplitude. In a multilayer thin film with n layers, the relationship between amplitude and displacement/stress is defined by the coefficient matrix $[D]$, which can be expressed by Equation (4).

$$\begin{Bmatrix} A_L^+ \\ A_L^- \\ A_S^+ \\ A_S^- \end{Bmatrix}_{ln} = [D]_{ln,t}^{-1}[D]_{ln-1,b}[D]_{ln-1,t}^{-1} \cdots [D]_{l1,b}[D]_{l1,t}^{-1} \cdot \begin{Bmatrix} u_x \\ u_z \\ \sigma_{zz} \\ \sigma_{xz} \end{Bmatrix}_{l1.t} \quad (4)$$

Here, the coefficient matrix of bottom and top interfaces are represented by b and t subscripts. Applying the transfer matrix method, the *SAW* velocity according to the thickness and frequency of the thin film can be derived.

2.2. Modeling the Adhesion Interlayer

The dispersion characteristics algorithm in Section 2.1 managed to derive the theoretical dispersion curve in the perfect bonding state between the thin film and the substrate. However, for the actual thin film deposited, variables such as properties of the substrate and the thin film, process equipment used, pretreatment conditions, and the deposition parameters determine the adhesion properties of the interface. Therefore, there will be some discrepancies between the theoretically calculated results and the actual results. In order to accurately evaluate the properties of the micro/nano-scale thin films, it is necessary to derive the dispersion characteristics considering the adhesion properties between the thin film and the substrate.

In order to consider the imperfect bonding state existing in the actual specimen, the adhesion properties were evaluated by modeling a virtual interface that has a spring stiffness coefficient value [4,17–19]. If the displacement of the interface in the perfect bonding state is Δu_p, and the displacement in the imperfect bonding state where defects or porosity exist at the interface is Δu_I, the total displacement, Δu_T, can be expressed as follows, when tensile or compressive stress is applied. Equation (5) is derived displacement focusing on the state of adhesive properties, and other parameters are not considered.

$$\Delta u_T = \Delta u_P + \Delta u_I \tag{5}$$

At the imperfect bonding state, the stiffness coefficient of the interface between the thin film and the substrate under a stress condition can be expressed as in Equation (6) below.

$$k = \sigma / \Delta u_I \tag{6}$$

It was theoretically confirmed that the more imperfect the bonding state was, the larger the displacement and the smaller the spring stiffness coefficient. In the thin film structure, the correlation between the stiffness coefficient and the adhesion force was identified through quasi-static modeling based on the fracture mechanics [17]. In order to apply the stiffness coefficient of the interface defined in Equation (6) to the dispersion characteristic simulation, the velocity of the longitudinal and transverse waves, respectively, can be expressed as follows.

$$C_L = \sqrt{\frac{K_N d_i}{\rho_i}}, \quad C_S = \sqrt{\frac{K_T d_i}{\rho_i}} \tag{7}$$

In Equation (7), K_N and K_T represent the stiffness coefficients in the normal and tangential directions, and d_i and ρ_i represent the thickness and density of the interfacial layer. The thickness of the bonding interface layer was set to 4% of the thickness of the thin film and the density was set to 11% of the lowest density among the thin film and the substrate [4]. Through this, the transverse and longitudinal wave velocities of the ultrasonic wave traveling through the interfacial layer can be calculated with the spring stiffness coefficient. The dispersion characteristic simulation considering the bonding layer model can be derived as Equation (8) by modifying Equation (4).

$$\begin{Bmatrix} A_L^+ \\ A_L^- \\ A_S^+ \\ A_S^- \end{Bmatrix}_{ln} = [D]_{sub,t}^{-1}[D]_{Inter,b}[D]_{Inter,t}^{-1}[D]_{film,b}[D]_{film,t}^{-1} \cdot \begin{Bmatrix} u_x \\ u_z \\ \sigma_{zz} \\ \sigma_{xz} \end{Bmatrix}_{l1.t} \tag{8}$$

Here, the sub, inter, and film denoted by subscripts represent substrates, inter-layer, and thin films. In order to derive the dispersion characteristics according to the stiffness coefficient of the bonding interface, five levels of adhesion strength were established, as

shown in Table 1. The dispersion curve derived by performing the dispersion characteristic simulation according to the adhesion level set in Table 1 is shown in Figure 2.

Table 1. Stiffness coefficient according to the bonding interface condition of multilayer thin film.

Interfacial Condition	Boundary Stiffness 10^{16} N/m^3	Longitudinal Velocity (m/s)	Shear Velocity (m/s)
Perfect bond	Boundary continuity	-	-
Complete debonding	$K_N = 0,\ K_T = 0$	0	0
level 1	$K_N = 216.0,\ K_T = 61.44$	14,120	7530
level 2	$K_N = 54.0,\ K_T = 15.36$	7060	3770
level 3	$K_N = 13.5,\ K_T = 3.84$	3530	1880
level 4	$K_N = 3.38,\ K_T = 0.69$	1760	940
level 5	$K_N = 0.84,\ K_T = 0.24$	880	470

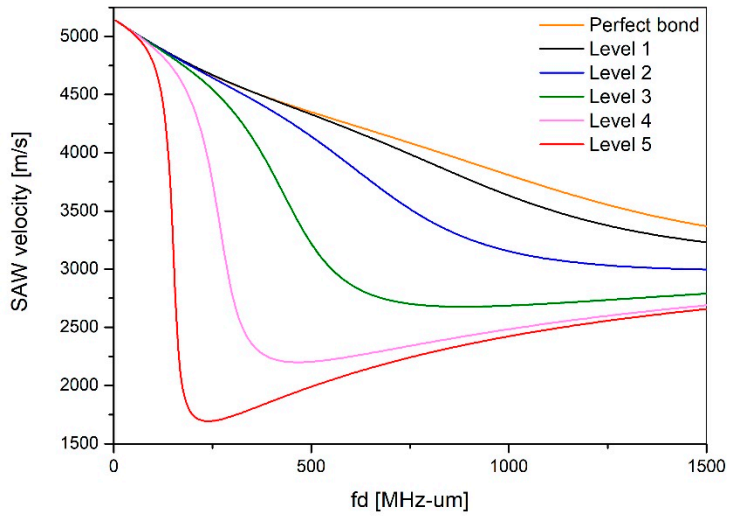


Figure 2. Dispersion curve simulation according to interface conditions.

The results show that the higher the stiffness coefficient is, the closer it is to the ideal dispersion curve in a perfect bonding state. Conversely, as the stiffness coefficient decreases, the thin film is assumed to be completely separated from the substrate, hence it converges to the dispersion curve of the lamb wave, which is a plate wave only within the thin film.

3. Experimental Setup and Method

3.1. Preparation of Specimen

Thin titanium film was deposited on a silicon wafer (100) using a DC magnetron sputtering equipment to derive the stiffness coefficient of the thin film through the dispersion simulation. The thickness of the thin film was deposited with a target of 600 nm. In the sputtering process, higher DC power increases the residual stress in the material and decreases the external load needed to fracture the interface, as well as the bonding force [20]. Therefore, in order to fabricate the specimens of different bonding strengths, the process was performed for five groups with different DC power levels, from 28.8 W to 144 W. Other deposition conditions were set as the same, except for DC Power. The other detailed deposition conditions are set at a chamber pressure of 5 Torr, a target distance of 7 cm, a flow rate of 15 sccm, and an operating pressure of 3.7 mTorr.

Since the dispersion characteristics of the *SAW* propagating through the thin film is greatly affected by the thickness of the thin film, an accurate thickness was measured by taking a cross section of the thin film using a scanning electron microscope (SEM). The measurements are as shown in Figure 3. From the cross-section images, it was found that the error was about 4.5% on average when compared to the initial target thickness of

600 nm. It appears that the error in thickness occurred due to a large variation in deposition rate depending on the deposition conditions.

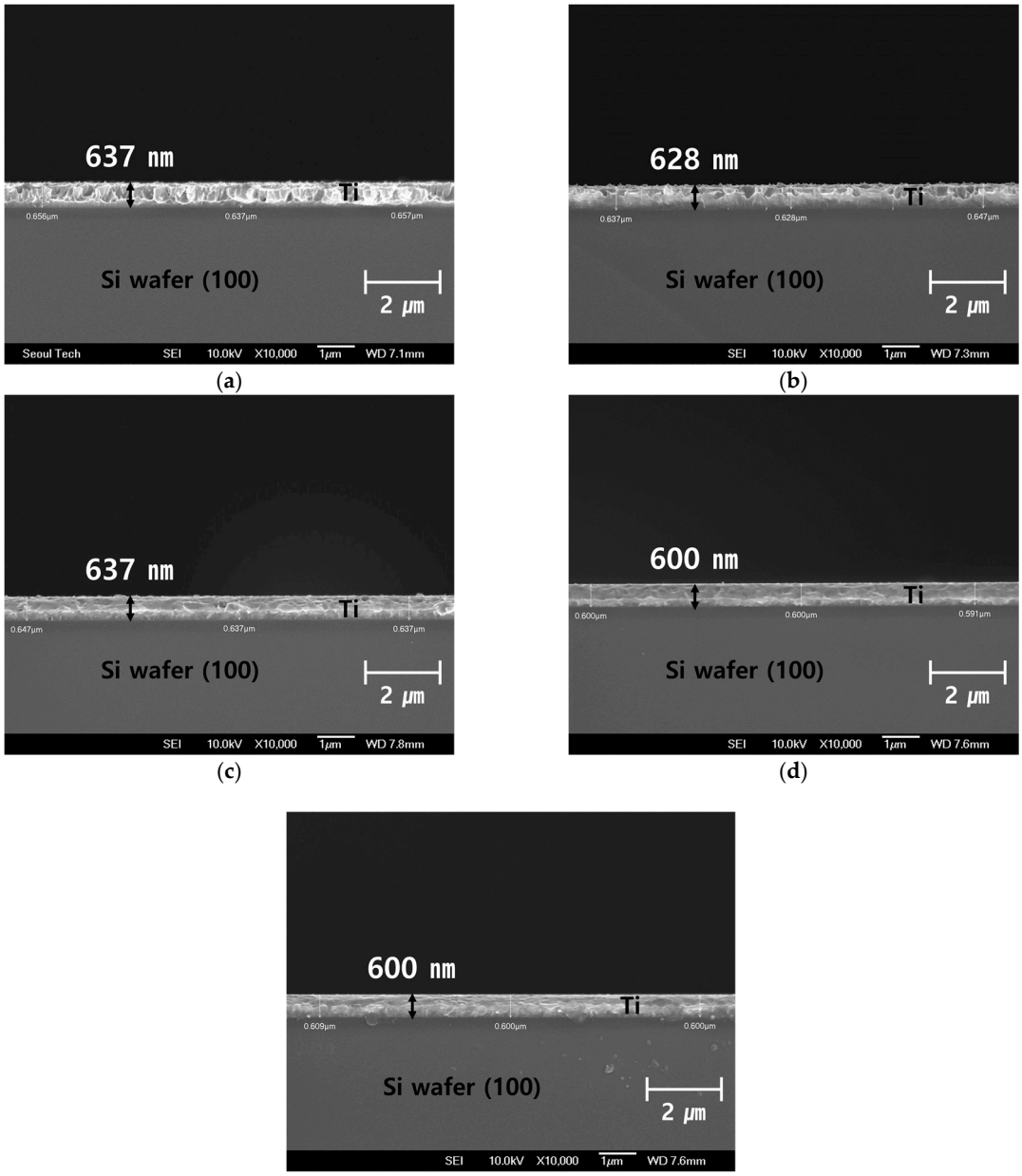


Figure 3. SEM image for Ti thin film thickness measurement: (**a**) 28.8 W; (**b**) 57.6 W; (**c**) 86.4 W; (**d**) 115.2 W; (**e**) 144 W.

3.2. Surface Acoustic Wave Velocity Measurement Using a Scanning Acoustic Microscope

The velocity of the *SAW* was measured using the *Vz* method of scanning acoustic microscope, which is widely used for non-destructive evaluation of material properties. The *Vz* method calculates the velocity of the *SAW* by superimposing the signals incident/reflected vertically and the leakage signals of *SAW* that are incident on the specimen at a second critical angle along the lens shape and propagated to the surface. The waveform of the signal along the defocused distance of the probe lens is called a *Vz* curve, and the

distance between signal peaks is defined as Δz. The velocity of the *SAW* is defined as in Equation (9) below.

$$C_{SAW} = C_W \left[1 - \left(1 - \frac{C_W}{2f \triangle z} \right)^2 \right]^{-1/2} \quad (9)$$

Here, C_W is the sound speed in the water, and f is the applied frequency. The *SAW* velocity was measured using a UH3 scanning acoustic microscope manufactured by Olympus, and a 200 MHz transducer was used as the applied frequency. The wave velocity was measured five times for each specimen, and the results are as shown in Figure 4. The averages of *SAW* velocity according to the test specimen production conditions are 4831 m/s at 28.8 W, 4777.2 m/s at 59.6 W, 4805 m/s at 86.4 W, 4731.2 m/s at 115.2 W, and 4701.4 m/s at 144 W.

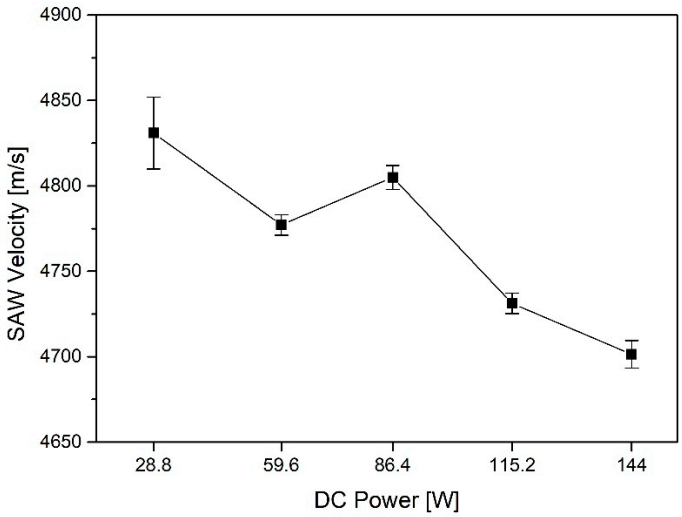


Figure 4. The results of *SAW* velocity using a scanning acoustic microscope (m/s).

As a result of measuring the *SAW* velocity of the Ti/Si specimen using a scanning acoustic microscope, it appeared that the higher DC power, the lower the wave velocity.

3.3. Evaluation of Stiffness Coefficient Using Dispersion Characteristics

The value of the stiffness coefficient for each specimen was quantitatively derived by comparing the dispersion curve according to the stiffness coefficient and the *SAW* velocity measured by the scanning acoustic microscope. On the dispersion curve divided by the 5 levels of stiffness coefficients, it was confirmed that the actual velocity of the *SAW* was distributed between the bonding levels 4 and 5. As a result of the simulation by subdividing the section, the stiffness coefficient was derived according to each velocity measurement value. The dispersion curves for each level are shown in Figure 5. In the figure, the dashed line means the subdivided dispersion curve and the stiffness coefficient corresponding to the measured *SAW* velocity can be derived. The results of the stiffness coefficients that correspond to the measured values of the *SAW* velocity of each specimen are as shown in Table 2.

Table 2. The results of the stiffness coefficients according to deposition condition.

Specimen	DC Power Condition(W)				
	28.8	**57.6**	**86.4**	**115.2**	**144**
K_N $(10^{16}$ N/m$^3)$	1.6065	1.1508	1.3125	1.0038	0.9429
K_T $(10^{16}$ N/m$^3)$	0.459	0.329	0.375	0.287	0.269

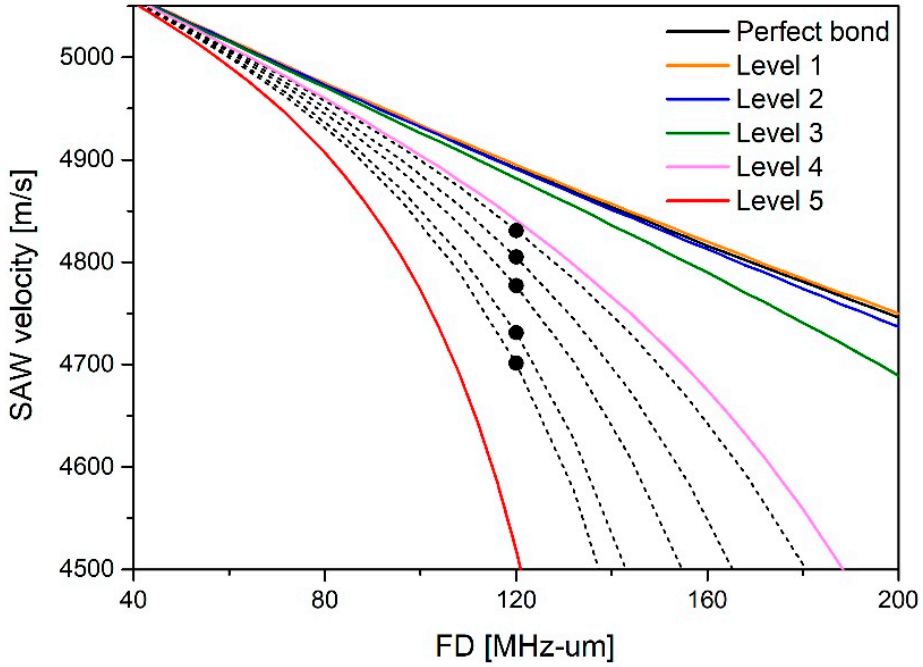


Figure 5. Results of *SAW* velocity on dispersion curve by interface condition.

3.4. Adhesion Force Evaluation by Nano-Scratch Test

NanoTest NTX, a commercialized nano-scratch equipment, was used to evaluate the quantitative adhesion force of the fabricated specimens. In the nano-scratch test, the critical load is the point where the thin film is completely debonded from the substrate and the work of adhesion is calculated by using the critical load [21]. The relationship between the work of adhesion and the critical load is as shown in Equation (10) below.

$$L_C = \frac{\pi d^2}{8}\left(\frac{2EW_{AD}}{t}\right)^{1/2} \tag{10}$$

In the equation, L_C is the critical load, d is the scratch width, W_{AD} is the work of adhesion, and E and t are the elastic modulus and thickness of the thin film.

In this study, since the same experimental conditions and materials were used, the work of adhesion is proportional to the critical load. Thus, the critical load measured from the nano-scratch test was expressed in terms of the adhesion force. The experimental conditions were set as shown in Table 3 below. The nano-scratch test was conducted five times for each specimen, and the load value at the point of interfacial failure was recorded by red dashed line with the optical microscope, as shown in Figure 6.

Table 3. Experimental condition of nano-scratch test.

Tip Type	5 μm Sphero-Conical
Initial load (mN)	0.01
Final load (mN)	300
Loading rate (mN/s)	2.5
Speed (μm /s)	2
Length (μm)	350

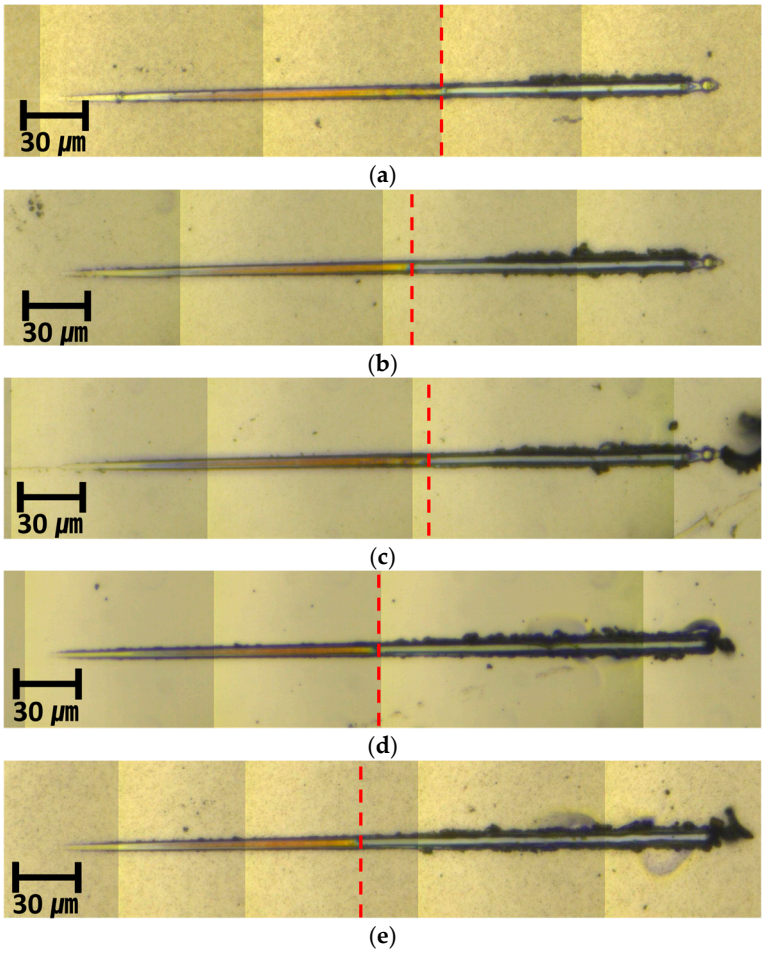


Figure 6. Nano-scratch test OM image: (**a**) 28.8 W; (**b**) 57.6 W; (**c**) 86.4 W; (**d**) 115.2 W; (**e**) 144 W.

As the results in Figure 7 indicate, the critical load tends to decrease when the DC power, a deposition condition, increases.

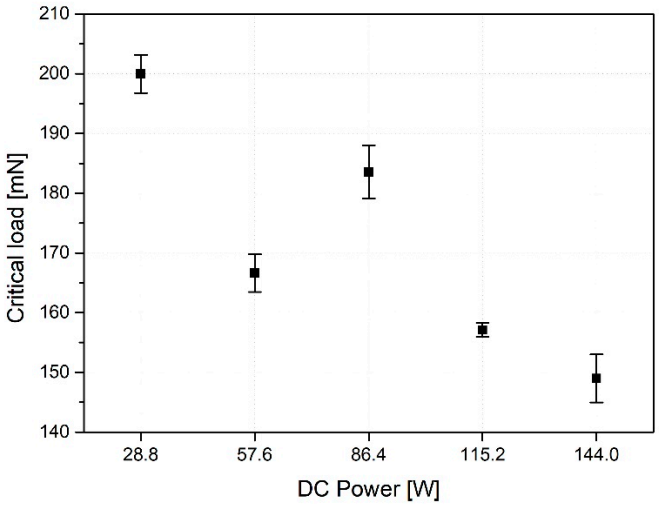


Figure 7. The results of critical load by nano-scratch test [mN].

4. Conclusions

In this study, in order to evaluate the adhesion properties of thin film structures, the stiffness coefficients were derived by the dispersion characteristics of the *SAW*, and the reliability of the results was verified through the nano-scratch test. Table 4 shows the results of the stiffness coefficients from the dispersion characteristics and the results of the adhesion forces derived through the nano-scratch test. From the comparative evaluation of the stiffness coefficient and the adhesion force of the specimens according to the deposition condition, it was confirmed that the trends of the results were very similar. Through this, we confirmed the reliability of the dispersion characteristic simulation technique to evaluate the adhesion properties of thin films in this study.

Table 4. The compared result to the stiffness constants and the critical load.

Specimen		DC Power Condition (W)				
		28.8	**57.6**	**86.4**	**115.2**	**144**
Stiffness constant $(10^{16}\ \mathrm{N/m^3})$	K_N	1.6065	1.1508	1.3125	1.0038	0.9429
	K_T	0.459	0.329	0.375	0.287	0.269
Critical load (mN)		199.95	166.61	183.57	157.11	148.99

Author Contributions: Conceptualization, Y.M.C. and D.K.; Data curation, Y.M.C.; Formal analysis, Y.M.C. and D.K.; Funding acquisition, I.K.P.; Investigation, Y.M.C.; Methodology, Y.M.C. and D.K.; Project administration, I.K.P.; Validation, Y.M.C., D.K. and J.N.K.; Visualization, Y.M.C.; Writing—original draft, Y.M.C. and I.K.P.; Writing—review & editing, D.K., J.N.K. and I.K.P. All authors have read and agreed to the published version of the manuscript.

Funding: This study was supported by the Research Program funded by the Seoul Tech (Seoul National University of Science and Technology), grant number 2022-0650.

Institutional Review Board Statement: Not applicable.

Informed Consent Statement: Not applicable.

Data Availability Statement: Not applicable.

Conflicts of Interest: The authors declare no conflict of interest.

References

1. Mittal, K.L. Adhesion measurement of thin films. *Electrocompon. Sci. Technol.* **1976**, *3*, 21–42. [CrossRef]
2. Park, T.S.; Kwak, D.R.; Park, I.K.; Miyasaka, C. Evaluation of adhesive strength for nano-structured thin film by scanning acoustic microscope. *J. Korean Soc. Nondestruct. Test.* **2012**, *32*, 393–400. [CrossRef]
3. Tomastik, J.; Ctvrtlik, R.; Drab, M.; Manak, J. On the importance of combined scratch/acoustic emission test evaluation: SiC and SiCN thin films case study. *Coatings* **2018**, *8*, 196. [CrossRef]
4. Du, J.; Tittmann, B.R.; Ju, H.S. Evaluation of film adhesion to substrates by means of surface acoustic wave dispersion. *Thin Solid Films* **2010**, *518*, 5786–5795. [CrossRef]
5. Steinmann, P.A.; Tardy, Y.; Hintermann, H.E. Adhesion testing by the scratch test method: The influence of intrinsic and extrinsic parameters on the critical load. *Thin Solid Films* **1987**, *154*, 333–349. [CrossRef]
6. Othman, M.F.; Bushroa, A.R.; Abdullah, W.N.R. Evaluation techniques and improvements of adhesion strength for TiN coating in tool applications: A review. *J. Adhes. Sci. Technol.* **2015**, *29*, 569–591. [CrossRef]
7. Rahmati, B.; Sarhan, A.A.; Zalnezhad, E.; Kamiab, Z.; Dabbagh, A.; Choudhury, D.; Abas, W.A.B.W. Development of tantalum oxide (Ta-O) thin film coating on biomedical Ti-6Al-4V alloy to enhance mechanical properties and biocompatibility. *Ceram. Int.* **2016**, *42*, 466–480. [CrossRef]
8. Grossmann, M.; Schubert, M.; He, C.; Brick, D.; Scheer, E.; Hettich, M.; Gusev, V.; Dekorsy, T. Characterization of thin-film adhesion and phonon lifetimes in Al/Si membranes by picosecond ultra-sonics. *New J. Phys.* **2017**, *19*, 053019. [CrossRef]
9. Robin, M.; Jenot, F.; Ouaftouh, M.; Duquennoy, M. Influence of the laser source position on the generation of Rayleigh modes in a layer-substrate structure with varying degrees of adhesion. *Ultrasonics* **2020**, *102*, 106051. [CrossRef]
10. Jenot, F.; Fourez, S.; Ouaftouh, M.; Duquennoy, M. Nondestructive testing of thin films using surface acoustic waves and laser ultrasonics. *AIP Conf. Proc.* **2018**, *1949*, 230031.

11. Rajanna, P.M.; Luchkin, S.; Larionov, K.V.; Grebenko, A.; Popov, Z.I.; Sorokin, P.B.; Danilson, M.; Bereznev, S.; Lund, P.D.; Nasibulin, A.G. Adhesion of single-walled carbon nanotube thin films with different materials. *J. Phys. Chem. Lett.* **2020**, *11*, 504–509. [CrossRef]
12. Aijaz, A.; Ferreira, F.; Oliveira, J.; Kubart, T. Mechanical properties of hydrogen free diamond-like carbon thin films deposited by high power impulse magnetron sputtering with Ne. *Coatings* **2018**, *8*, 385. [CrossRef]
13. Park, T.S.; Choi, Y.M.; Cho, B.S.; Park, I.K. Analysis of Dispersion Characteristics of Rayleigh Waves in Nanostructured Thin Films. *Korean Soc. Nondestruct. Test* **2018**, *38*, 98–106. [CrossRef]
14. Lowe, M.J. Matrix techniques for modeling ultrasonic waves in multilayered media. *IEEE Trans. Ultrason. Ferroelectr. Freq. Control* **1995**, *42*, 525–542. [CrossRef]
15. Haskell, N.A. The dispersion of surface waves on multilayered media. *Bull. Seismol. Soc. Am.* **1953**, *43*, 17–34. [CrossRef]
16. Tian, R.; Nie, G.; Liu, J.; Pan, E.; Wang, Y. On Rayleigh waves in a piezoelectric semiconductor thin film over an elastic half-space. *Int. J. Mech. Sci.* **2021**, *204*, 106565. [CrossRef]
17. Baik, J.M.; Thompson, R.B. Ultrasonic scattering from imperfect interfaces: A quasi-static model. *J. Nondestruct. Eval.* **1984**, *4*, 177–196. [CrossRef]
18. Kumar, S.A.; Sudheer, G. Influence of the oxide layer on the quality of bonding in adhesively bonded metallic structures by ultrasonic guided waves. *Int. J. Adhes. Adhes.* **2021**, *111*, 102981. [CrossRef]
19. Le Crom, B.; Castaings, M. Shear horizontal guided wave modes to infer the shear stiffness of adhesive bond layers. *J. Acoust. Soc. Am.* **2010**, *127*, 2220–2230. [CrossRef]
20. Tanabe, H.; Miyoshi, Y.; Takamatsu, T.; Sugiura, H. Effects of bias voltage and discharge current on mechanical properties of TiN film deposited by DC magnetron sputtering. *J. Soc. Mater. Sci. Jpn.* **2003**, *52*, 143–148. [CrossRef]
21. Burnett, P.J.; Rickerby, D.S. The relationship between hardness and scratch adhesion. *Thin Solid Films* **1987**, *154*, 403–416. [CrossRef]